

# Spatial variability of surface mass balance along a traverse route from Zhongshan station to Dome A, Antarctica

DING Minghu,<sup>1,2,3,4</sup> XIAO Cunde,<sup>1,3</sup> LI Yuansheng,<sup>5</sup> REN Jiawen,<sup>1</sup> HOU Shugui,<sup>1,6</sup>  
JIN Bo,<sup>7</sup> SUN Bo<sup>5</sup>

<sup>1</sup>State Key Laboratory of Cryospheric Sciences, Cold and Arid Regions Environmental and Engineering Research Institute, Chinese Academy of Sciences, 320 Donggang West Road, Lanzhou 730000, China

E-mail: cdxiao@lzb.ac.cn

<sup>2</sup>Division of Cenozoic Geology and Environment, Institute of Geology and Geophysics, Chinese Academy of Sciences, Beijing 100029, China

<sup>3</sup>Institute of Climate System, Chinese Academy of Meteorological Sciences, 46 Zhongguancun South Avenue, Beijing 100081, China

<sup>4</sup>Graduate University of Chinese Academy of Sciences, Beijing 100049, China

<sup>5</sup>Polar Research Institute of China, Shanghai 200136, China

<sup>6</sup>Key Laboratory for Coast and Island Development, Ministry of Education School of Geographic and Oceanographic Sciences, Nanjing University, Nanjing 210093, China

<sup>7</sup>Chinese Arctic and Antarctic Administration, Beijing 100860, China

**ABSTRACT.** Stakes at 2 km intervals were installed in January 1997 and remeasured in February 1998, January 1999, January 2005 and during the 2007/08 austral summer along a 1248 km traverse route from Zhongshan station to Dome A, East Antarctica. Based on topographical parameters, meteorological features and the records of ~650 stakes and six stake arrays, the route is divided into five zones. We find that the snow accumulation rate decreases with increasing altitude as one progresses inland, except in the zone 800–1128 km from the coast, where the average annual accumulation rate is higher than in the zone 524–800 km from the coast. The Dome A zone (1128–1248 km) has the lowest accumulation rate ( $35 \text{ kg m}^{-2} \text{ a}^{-1}$ , 2005–08) due to having the highest elevation and being furthest from the coast. The surface mass balance in the region 202–1128 km from the coast exhibits no temporal change from 1999–2005 to 2005–08, but there is a change in the accumulation distribution. The zone from 202 to 524 km shows a decrease in surface mass balance from  $84 \text{ kg m}^{-2} \text{ a}^{-1}$  in 1999–2005 to  $67 \text{ kg m}^{-2} \text{ a}^{-1}$  in 2005–08, while the zone between 800 and 1128 km shows an increase from  $67 \text{ kg m}^{-2} \text{ a}^{-1}$  in 1999–2005 to  $75 \text{ kg m}^{-2} \text{ a}^{-1}$  in 2005–08.

## 1. INTRODUCTION

As stated by Solomon and others (2007), there is strong evidence that the global mean sea level gradually increased during the 20th century. Furthermore, it is projected to continue to rise at an even greater rate during the 21st century. The two major contributors to global sea-level rise are thermal expansion of the oceans and the loss of land-based ice due to increased melting. The total contribution of glaciers, ice caps and ice sheets to sea-level rise has been estimated at  $1.2 \pm 0.4 \text{ mm a}^{-1}$  for the period 1993–2003 (Solomon and others, 2007). The coastal regions of the ice sheets of Greenland and Antarctica, as well as the glaciers over the Antarctic Peninsula, play a substantial role in this trend.

Despite much debate on the topic (e.g. Jacobs and others, 1992; Ren and others, 2002a; Solomon and others 2007), there is still no conclusion as to whether or not the Antarctic ice sheet will maintain its stable and cold state under a climate-warming scenario. If dynamical properties such as ice-shelf collapse dominate the mass balance of the Antarctic ice sheet, a net loss may occur in the future. It is necessary to determine the surface mass-balance (SMB) conditions to estimate the present state of the ice sheet. Snow accumulation patterns are mainly influenced by air temperature, elevation, distance from the coast and wind-driven processes. To acquire knowledge of the SMB,

investigations of the spatial variability of snow accumulation are required.

Surface morphology at the metre scale (e.g. sastrugi) could influence firn-core and stake records on scales ranging from seasonal to multi-annual because of its variability in space (<1 km) and time (seasonal) (Frezzotti and others, 2007). Slope, wind direction and wind speed have a significant impact on SMB. A surface slope (determined by ice dynamics and bedrock topography) of  $<1 \text{ m km}^{-1}$  will accelerate katabatic winds, influencing wind-driven ablation processes and causing highly variable snow accumulation at intermediate scales between 1 and 20 km, even influencing intermediate-depth core records (Frezzotti and others, 2002b, 2005). On the Antarctic plateau, for a slope of  $>4 \text{ m km}^{-1}$  in the direction of prevailing winds, the snow accumulation rate is typically zero or even below zero (Frezzotti and others, 2002a). SMB on regional scales (~20 km or larger) is influenced by ice-sheet morphology (Frezzotti and others, 2007; Urbini and others, 2008), which is determined by the accumulation rate history, its spatial pattern and atmospheric boundaries.

In the past few decades, many techniques (e.g. stake measurements, ultrasonic sounders and snow physical/chemical reference layers (snow pits, firn/ice cores and radar profiles)) have been used to measure the SMB (Eisen and others, 2008). Of these methods, stake measurements

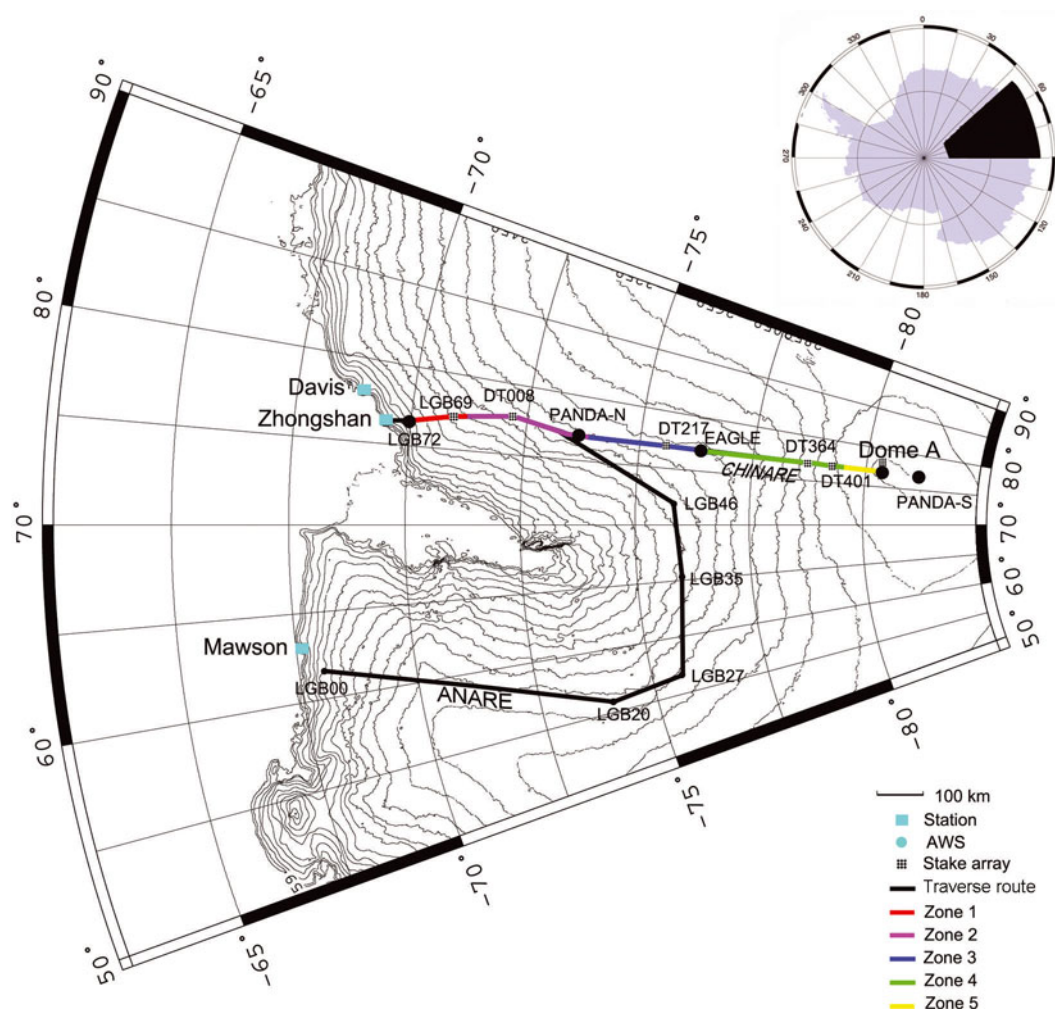


Fig. 1. Map of the traverse area and location of stake arrays and AWSs.

are accurate at a single site, but the shortcoming is that for long-term measurements and vast study regions, heavy logistical support is required.

In the 1996/97 austral summer, the first Chinese contribution to the International Trans-Antarctic Scientific Expedition (ITASE) was carried out by the Chinese National Antarctic Research Expedition (CHINARE), which travelled from Zhongshan station to 300 km inland (Fig. 1). One of the projects was to study the present SMB along the traverse route. CHINARE conducted four remeasurements up to 2008, reaching the summit of Dome A in 2005, and repeating the same traverse from Zhongshan to Dome A in 2008 (e.g. Ren and others, 2001, 2002a,b; Xiao and others, 2005). Six stake arrays were established along the traverse route during the 1999/2000 austral summer (except at Dome A) and were resurveyed from one to three times during the period 2001–08. Based on the data acquired, preliminary results were published (Ren and others, 2001, 2002a,b; Xiao and others, 2005), but no systematic research across the whole profile has been reported. Here we study the overall spatial characteristics of the SMB along the traverse route and conduct a few simple temporal analyses.

## 2. METHODOLOGY

The traverse route starts at Zhongshan and ends at the Dome A summit, covering a distance of 1248 km (Fig. 1). The

transect is located on the eastern side of the Lambert Glacier basin (LGB), approximately along longitude 77° E. Lambert Glacier lies in a deep rift valley in the East Antarctic ice sheet, with ice flow converging into the glacier and draining into the Amery Ice Shelf (Xiao and others, 2005).

Bamboo poles with ~3.5 m exposed, ~1.5 m inserted into the snow and 2–3 cm in diameter, were measured at 2 km intervals along the route. During 1992–94, the Australian National Antarctic Research Expeditions (ANARE) performed measurements along the LGB72–LGB35–LGB00 route, overlapping the initial 300 km of the CHINARE route in the east LGB (Fig. 1). CHINARE set up 114 stakes along the initial 336 km in January 1997. In February 1998, all stakes were remeasured, and another 119 were installed. In January 1999, another 352 stakes were installed. In January 2005, all remaining stakes were remeasured and replaced along the 1248 km route, and 78 extra stakes were installed to fill blanks. During the 2007/08 season, 587 stakes were remeasured (some were lost or damaged).

Six stake arrays were set up during January 1998, January 1999 and January 2005 along the transect (Xiao and others, 2005), each including 36 stakes planted in a 6 × 6 matrix over a 100 m × 100 m area (25 stakes at Dome A). The stakes are spaced at ~20 m intervals. Table 1 shows details of these arrays.

Surface snow densities of the upper 0.2 m were measured at 10 km intervals over the entire 1248 km of the traverse

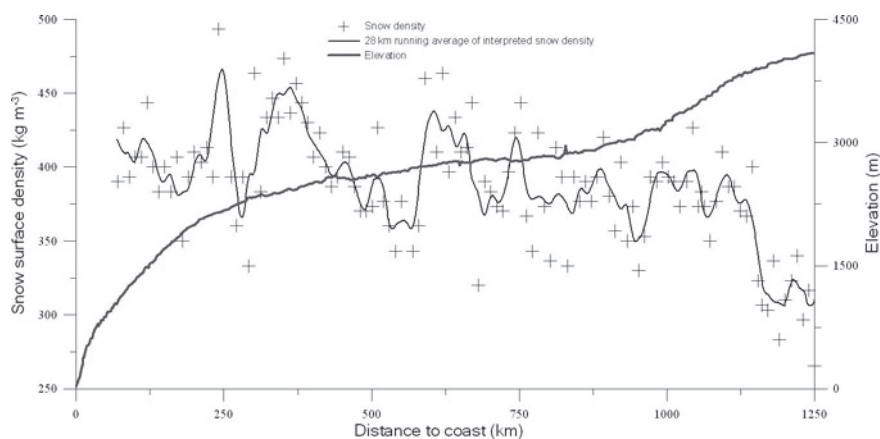


Fig. 2. Density profile of surface snow along CHINARE traverse route.

route from Zhongshan to Dome A during the 2007/08 season using a simple weight–volume measurement method. The density values were interpolated, then smoothed by a 28 km running average to remove spatial and measurement noise (Fig. 2). The estimated measurement accuracy is 95%. The average density is  $389 \text{ kg m}^{-3}$ , varying from  $460 \text{ kg m}^{-3}$  under the influence of katabatic winds on the near-coastal slopes (250–600 km from the coast) to  $310 \text{ kg m}^{-3}$  in the Dome A area, where the main form of precipitation is diamond dust (Hou and others, 2007). A preferred method was introduced by Takahashi and Kameda (2007) who considered the snow densification process in the time interval between stake measurements, but no vertical density profiles are available. Our SMB may thus tend to be an underestimate.

### 3. MORPHOLOGICAL AND METEOROLOGICAL CHARACTERISTICS

There are five automatic weather stations (AWSs) along the traverse route: LGB69 (170 km from the coast; installed in 2002), PANDA-N (501 km; installed in 2008), EAGLE (806 km; installed in 2005), Dome A (1228 km; installed in 2005) and PANDA-S (1350 km; installed in 2008). Continuous meteorological data have been recorded at Zhongshan since 1989 (Ma and others, 2010). Data from these stations demonstrate that the annual average wind speed

increases inland from Zhongshan ( $7.0 \text{ m s}^{-1}$ ) to LGB69 ( $9.5 \text{ m s}^{-1}$ ) and then decreases from PANDA-N ( $\sim 8 \text{ m s}^{-1}$ ) to EAGLE ( $3.9 \text{ m s}^{-1}$ ) to Dome A ( $2\text{--}3 \text{ m s}^{-1}$ ). The seasonal variability decreases inland. Dome A, the summit of the East Antarctic ice sheet ( $80^{\circ}22'01.63'' \text{ S}$ ,  $77^{\circ}22'22.90'' \text{ E}$ ;  $4092.46 \text{ m a.s.l.}$ ; Zhang and others, 2007), is especially free of the influence of katabatic winds because of its low slope and high altitude. Ding and others (2010) measured 10 m firn temperature by thermistor and found that it is strongly correlated with distance from the coast and surface elevation (Table 2), with a near-dry-adiabatic lapse rate ( $1.2^{\circ}\text{C}(100 \text{ m})^{-1}$ ,  $R^2 = 0.98$ ), less than on the western side of the LGB, where weaker winds and lower annual mean temperatures prevail (Allison, 1998). The value of near-dry-adiabatic lapse rate using 10 m firn temperature is close to that using AWS data ( $\sim 1^{\circ}\text{C}(100 \text{ m})^{-1}$ ; Ma and others, 2010). The middle part of this transect is topographically inclined westwards (Ren and Qin, 1995; Xiao and others, 2005), making the prevailing wind direction east; between the coast and Dome A the wind changes direction from east-northeast to northeast, to south-southeast to northeast, and then east to south. Simulations of the moisture transport mechanism over the LGB by Connolley and King (1996) and Slonaker and Van Woert (1999) show that the eastern side of the LGB receives more vapour than the western side (probably because air masses flow through the eastern side easily due to the relatively flat topography over the coast). Using 1994–96

Table 1. Location of the stake arrays and compilation of the accumulation rates and temperature data

Stake array	Lat. (S)	Long. (E)	Inst.	1st re meas.	2nd re meas.	Dist.	Elev.	<i>T</i>	Acc.			
									Inst.–1st	1st–2nd	Inst.–2nd	Inst.–2nd
						km	m a.s.l.	°C	$\text{kg m}^{-2} \text{ a}^{-1}$	$\text{kg m}^{-2} \text{ a}^{-1}$	$\text{kg m}^{-2} \text{ a}^{-1}$	%
LGB69*	$70^{\circ}50'$	$77^{\circ}4'$	Jan 1999	Jan 2002	–	170	1900	–28.2	286	–	–	–
DT008	$72^{\circ}1'$	$77^{\circ}56'$	Dec 1998	Feb 2005	Jan 2008	310	2390	–33.6 <sup>†</sup>	138	80	118	30
DT217	$75^{\circ}43'$	$76^{\circ}50'$	Dec 1998	Jan 2005	Jan 2008	728	2800	–41.3 <sup>†</sup>	11	12	12	172
DT364	$78^{\circ}20'$	$77^{\circ}0'$	Jan 1999	Jan 2005	Jan 2008	1022	3380	–48.0 <sup>†</sup>	56	72	62	14
DT401	$79^{\circ}0'$	$77^{\circ}0'$	Jan 1999	Jan 2005	Jan 2008	1097	3675	–50.6 <sup>†</sup>	25	28	26	48
Dome A	$80^{\circ}22'$	$77^{\circ}21'$	Jan 2005	Jan 2008	Jan 2009	1228	4093	–58.2	18	21	19	25

Notes: Inst.: Installation date; re meas.: remeasurement date; Dist.: Distance to coast along the traverse; Elev.: Elevation (World Geodetic System 1984 (WGS84) ellipsoid); *T*: 10 m firn temperature; Acc.: Accumulation rate.

\*Results from Xiao and others (2005).

<sup>†</sup>Results from regression analyses plus kriging interpolation (Ding and others, 2010).

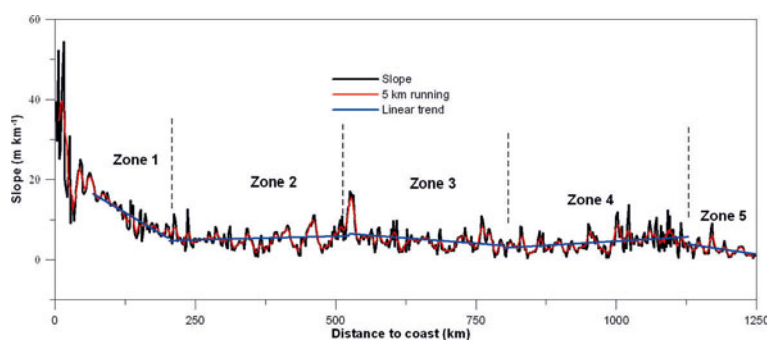


**Fig. 3.** Transect slope profile and the different sections along the CHINARE traverse route.

AWS data, Allison (1998) reported that the accumulation rate on the eastern side of the LGB ( $65 \text{ kg m}^{-2} \text{ a}^{-1}$  at LGB59) is up to 50% lower than that at equivalent elevations ( $\sim 2600 \text{ m}$ ) on the western (windward) side ( $129 \text{ kg m}^{-2} \text{ a}^{-1}$  at LGB10), since the area is in the 'rain shadow' of the prevailing upper-level winds. Strangely, recent observations have indicated an opposite condition: measured accumulation rates higher on the eastern side of the LGB ( $199 \text{ kg m}^{-2} \text{ a}^{-1}$  at LGB69 for 2002–03; Ma and others, 2010) than at equivalent elevations ( $1850 \text{ m}$ ) on the western side ( $97 \text{ kg m}^{-2} \text{ a}^{-1}$  at LGB00 for 1994–96).

Wind-driven processes have a great impact on SMB. Strong winds cause snowdrifts, and the constancy of wind direction decides the local variability. Sastrugi are produced by wind erosion of snow redistribution, reflecting wind speed and direction, post-deposition processes and local variations in SMB (Goodwin, 1991). We sorted sastrugi by height and amount in unit area in January 2005, and obtained results varying slightly from those of Ren and others (2001). The principal heights of sastrugi exhibit a narrow range along the whole traverse, except in the Dome A area where the sastrugi height is 30–60 cm. In the near-coastal 250 km region, sastrugi occur more frequently and are higher than 60 cm, with lengths of 2–5 m and intervals of several metres. Especially in the ice-divide area from 900 to 1128 km, the number of sastrugi increases tremendously from  $\sim 40 \text{ km}^{-1}$  to  $>130 \text{ km}^{-1}$ . The predominant slope direction also changes from  $\sim 240^\circ$  to  $\sim 100^\circ$ . The coastal

and slope areas are dominated by varying directions due to the presence of katabatic and barrier winds, which present different prevalent directions. Inland, winds are predominantly katabatic, and seasonal variability is reduced. Sastrugi are sparser and shorter, except near ice divides, where the sastrugi length and interval increase to tens of metres because the slope is opposite to the wind direction.

We calculated surface slope from the digital elevation model (DEM) developed by the US National Snow and Ice Data Center. The transect shows an overall positive slope from LGB72 to Dome A (Figs 1 and 3) that can be classified into five zones according to slope and morphological conditions (Fig. 3; Table 3).

**Zone 1:** steeply sloping area; a sector of steep but decreasing slope, from 68 km (LGB72) to 202 km, with an average slope of  $11 \text{ m km}^{-1}$  (max.  $18 \text{ m km}^{-1}$ ) and the prevailing aspect towards the northwest.

**Zone 2:** slightly rising area; a sector with a slight altitude increase, from 202 to 524 km, with an average slope of  $5.4 \text{ m km}^{-1}$ , and the prevailing aspect towards the north-northwest.

**Zone 3:** extremely flat area; a stable sector of decreasing slope with a hard surface crust from 524 to 800 km, with an average slope of  $5.0 \text{ m km}^{-1}$  and short-distance decreases in elevation. The prevailing aspect is northwards. This section is the flattest ( $\sim 0.7 \text{ m km}^{-1}$ ) if the

**Table 2.** The 10 m firm temperature along CHINARE (Ding and others, 2010)

Site	Lat. °S	Long. °E	Elev. m a.s.l.	Dist. km	Temp. °C	Date
LGB69	70.8353	77.0747	1854	172	-27.2	2005–06
LT925	71.0954	77.2886	1996	202	-28.5	1994
LT910	71.3606	77.5112	2135	233	-30.7	1994
LT895	71.6205	77.7305	2214	263	-31.7	1994
LT880	71.8808	77.9509	2325	294	-33.1	1994
LT865	72.1505	77.9494	2351	324	-33.3	1994
LT850	72.4106	77.7231	2424	354	-34.7	1994
LT835	72.6712	77.4936	2468	384	-34.5	1994
LT805	73.1914	77.0268	2581	444	-36.1	1994
LT790	73.452	76.7877	2537	474	-36.1	1994
LT743	74.2595	76.1687	2476	564	-35.6	1994
LT730	74.4793	75.8756	2468	594	-35.5	1994
EAGLE	76.4197	77.0239	2830	801	-43.1	2005–08
Dome A	80.3675	77.3439	4093	1248	-58.2	2005–08

**Table 3.** Snow accumulation rate by sector and its relationship to the slope along the traverse

Dist. km	Average slope m km <sup>-1</sup>	Acc. 1997–98 kg m <sup>-2</sup> a <sup>-1</sup>	Acc. 1998–99 kg m <sup>-2</sup> a <sup>-1</sup>	Acc. 1999–2005 kg m <sup>-2</sup> a <sup>-1</sup>	Acc. 2005–08 kg m <sup>-2</sup> a <sup>-1</sup>	Std dev.2005–08 %	Acc. 1999–2008 kg m <sup>-2</sup> a <sup>-1</sup>
68–202	10.9	615	239	–	157	42	–
202–524	5.4	–	–	84	67	80	73
524–800	5.0	–	–	51	53	80	52
800–1128	4.3	–	–	67	75	59	72
1128–1246	2.6	–	–	–	35	54	–
202–1128	–	–	–	65.5	65.5	–	–
524–1128	–	–	–	59	65	–	–

Note: Not all records are reported here: for example, the data for the stakes from 204 to 292 km, which were installed or remeasured in 1997, 1998 and 1999, because they were not overlapped by the following traverses.

slope is calculated in the traverse direction, because this section is parallel to the elevation contour.

*Zone 4:* ice-divide area; this area extends from 800 to 1128 km, where the average slope (4.3 m km<sup>-1</sup>) is not high but the aspect changes greatly. Large basins with diameters from tens to thousands of metres were observed in this region.

*Zone 5:* Dome area; the Dome A area, spanning 1128–1248 km, with a gentle slope of ~2.6 m km<sup>-1</sup>.

## 4. RESULTS AND DISCUSSION

### 4.1. Local-scale (<1 km) spatial variability of surface mass balance

Stake heights vary due to solid precipitation, transport, sublimation and compaction of snow (Dibb and Fahnestock, 2004). Previous studies of accumulation patterns derived from stake array measurements have been carried out near Dome C and Talos Dome (Frezzotti and others, 2005, 2007). We can survey the spatial variability of SMB at stake arrays on an annual scale by comparing the accumulation measurements at each stake with the average across the stake array. The accumulation pattern, which reflects snow surface roughness, shows marked variability at these sites. The analyses of these stake arrays (Table 1; Fig. 4) suggest that local noise varies greatly on both temporal and spatial scales.

The surface morphologies are similar at LGB69 and DT008 according to our fieldwork, where wind crusts and sastrugi higher than 60 cm are occasionally observed because of strong wind and high precipitation. Sastrugi higher than 30 cm dominate at DT364 and DT401 (>1000 km from the coast). DT217 has a 'hard/tough' snow surface. The wind speed (3.9 m s<sup>-1</sup>) is a little higher at this site than at Dome A (2–3 m s<sup>-1</sup>), as is the annual mean wind directional constancy (0.91 versus 0.78; Ma and others, 2010). The slope (~350°) is oriented along the prevalent wind direction (northeast). The site contains well-developed wind crusts, and 31% of stakes indicate negative accumulation over a 9 year period. It can be deduced that, in this area, there is strong wind ablation (cf. site M2 along the Terra Nova Bay–Dome C transect; Frezzotti and others, 2005).

The accumulation distribution graph (Fig. 4) shows that most of the stakes have accumulation differences varying by >±10% from the average. Negative accumulation values were observed for individual stakes at DT008,

DT217, DT401 and Dome A. Negative values were also present at the relatively high-accumulation-rate site DT008 (118 kg m<sup>-2</sup> a<sup>-1</sup>). The multi-year average increases the representativeness of each stake array. This has been confirmed by Goodwin and others (2003), who suggested that the 3 year running mean accumulation data of the eastern Wilkes Land ice core are representative of the precipitation minus evaporation, whereas the 1 year accumulation data only reflect precipitation plus local noise. Analyses at the South Pole (McConnell and others, 1997) and on the traverse along Terra Nova Bay to Dome C (Frezzotti and others, 2005) have demonstrated a correlation between stake standard deviations and wind transport. We analysed the Gaussian distribution (Fig. 4) of annual accumulation values for 1999–2005 versus 2005–08 (at Dome A) from the stake arrays and found that the sites with lower accumulations had flatter stake value distributions and higher standard deviation, but there are different influencing factors. For instance, DT217 has the roughest morphology due to high ablation, whereas at Dome A the precipitation is the lowest, and the wind speed is low. The information (Table 1) at all sites shows that the lowest standard deviation values (14%) correspond to areas in which the wind speed is low and the post-redistribution process is weak (DT364). Although DT401 and DT364 are close to each other and under the control of similar air masses, the difference in their snow accumulation rates is large. This is mainly due to wind scouring, which is stronger at DT401 and is reflected in Figure 4, which shows 25% negative values for 2005–08. DT008 has an intermediate standard deviation (30%), due to high precipitation coupled with strong katabatic winds. DT217 shows extremely low accumulation values, even lower than at Dome A, and the highest standard deviation (172%). This site also has the largest number of stakes indicating ablation (28%). LGB69 is located on the escarpment of the route and exhibits low standard deviations (8%) even in an area of strong katabatic winds, due to high precipitation (75 cm (snow) a<sup>-1</sup>; ~285 kg m<sup>-2</sup> a<sup>-1</sup>; Xiao and others, 2005). An interesting phenomenon is that stakes indicating lower than average accumulation across the stake array will indicate higher accumulation later.

### 4.2. Regional-scale spatial variability of surface mass balance

Previous studies (Ren and Qin, 1995, 1996; Ren and others, 2001, 2002a,b; Xiao and others, 2005, 2008) have found that the coastal region has the highest accumulation rate and that

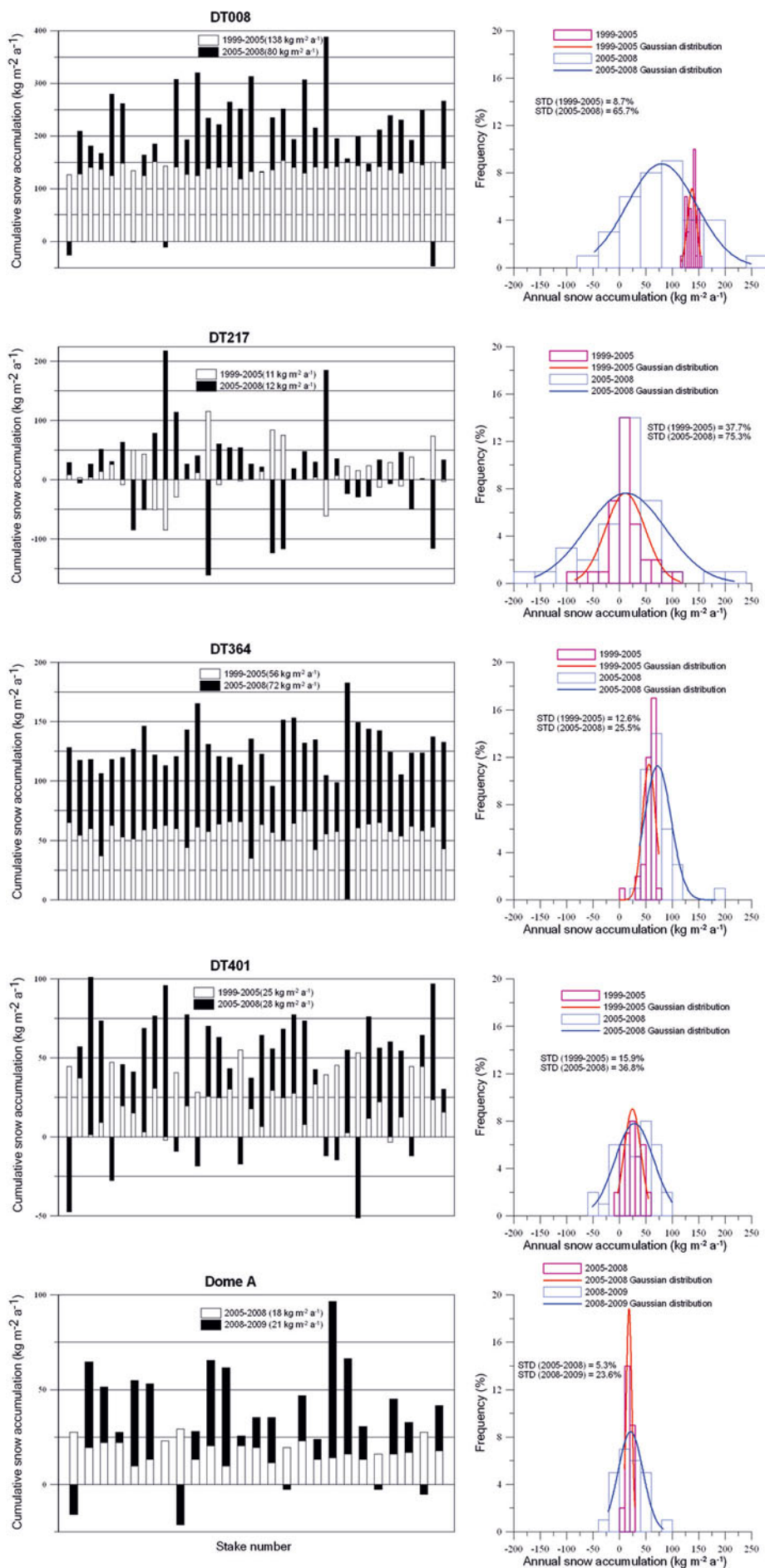


**Fig. 4.** Different accumulation/ablation patterns determined from the stake array measurements and frequency analyses of accumulation with respect to the annual average accumulation (STD is standard deviation).

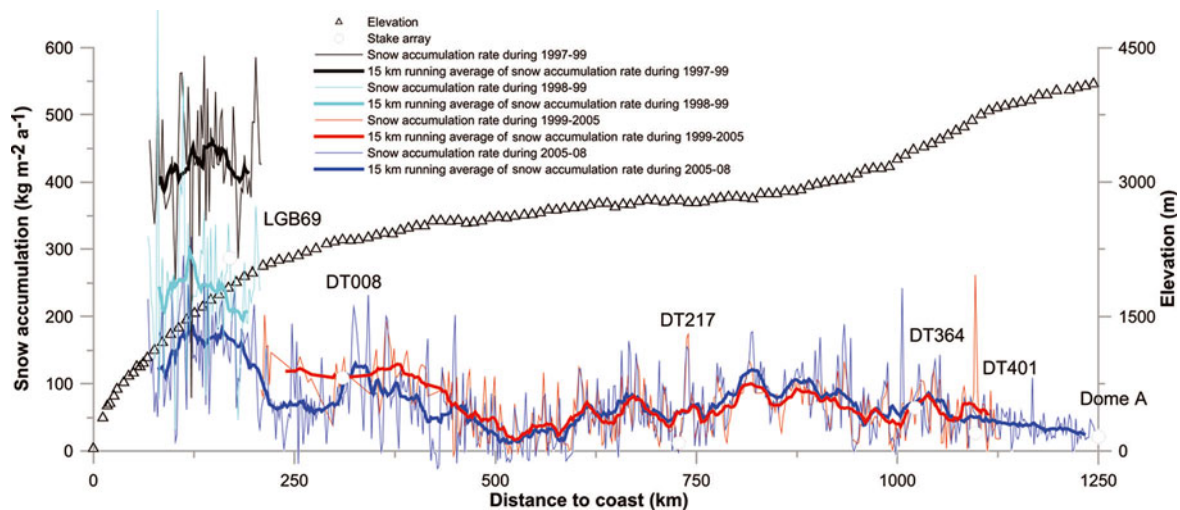


Fig. 5. The distribution of the SMB along the CHINARE traverse route.

the 200–300 km section of the traverse indicates low accumulation rates (this appears to be common in the East Antarctic ice sheet). The annual average snow accumulation over the initial 300 km was  $124 \text{ kg m}^{-2} \text{ a}^{-1}$  for the 1994 ANARE traverse, while an average of  $171 \text{ kg m}^{-2} \text{ a}^{-1}$  over the initial 460 km for 1998–99 was measured by CHINARE. The accumulation rate between the 460 and 1100 km sections was estimated to be  $70\text{--}180 \text{ kg m}^{-2} \text{ a}^{-1}$ , according to snow-pit results (Ren and others, 2001). Based on the horizon of  $\beta$  activity and density profiles, the accumulation rate at Dome A since 1964–65 is  $23 \pm 2 \text{ kg m}^{-2} \text{ a}^{-1}$  (Hou and others, 2007).

The SMB along the CHINARE route for 1997–2008 as determined by stake measurements is displayed in Figure 5. The figure shows a generally decreasing pattern from Zhongshan to Dome A, which is consistent with observations from other regions such as Terra Nova Bay–Dome C and Syova station–Dome Fuji (Furukawa and others, 1996; Frezzotti and others, 2005). From the figure, it is evident that the general accumulation rate is high near the coast and decreases inland until  $\sim 202$  km from the coast; it then increases until  $\sim 350$  km and decreases again until  $\sim 524$  km. The accumulation rate in the region from 524 to 800 km is stable and low. The ice-divide area from 800 to 1128 km also presents a slightly increasing trend of snow accumulation approaching the dome, where the lowest-accumulation area is located. Table 3 divides the traverse into five sections; in the discussion below, we use only the 2005–08 data for comparison.

**Zone 1:** The steeply sloping area (68–202 km) has an average accumulation rate of  $157 \text{ kg m}^{-2} \text{ a}^{-1}$  (39 cm of snow). The average slope is  $11 \text{ m km}^{-1}$ , and the precipitation is high, which may be the main reason for the low variability ( $13.5\text{--}318 \text{ kg m}^{-2} \text{ a}^{-1}$ ), with a standard deviation of 42%.

**Zone 2:** The slowly rising area (202–524 km) is characterized by an average accumulation rate of  $67 \text{ kg m}^{-2} \text{ a}^{-1}$  (16 cm of snow) and the highest variability ( $-26.5$  to  $232 \text{ kg m}^{-2} \text{ a}^{-1}$ ), with a standard deviation of 80%. On this section of the route the katabatic wind converges from the south-southeast and greatly influences the snow redistribution/erosion, producing a convex-up pattern (Fig. 5).

**Zone 3:** The region between 524 and 800 km presents wind speeds lower than in zone 2; however, the wind converges and induces many wind crusts. The average accumulation rate is  $53 \text{ kg m}^{-2} \text{ a}^{-1}$  (13 cm of snow), with high variability ( $-15$  to  $164 \text{ kg m}^{-2} \text{ a}^{-1}$ ) and a standard deviation of 80%.

**Zone 4:** The average accumulation rate of  $75 \text{ kg m}^{-2} \text{ a}^{-1}$  (20 cm of snow) in the ice-divide area (800–1128 km) is higher than that of zone 3, even though it is further from the coast, and there is a moderate variability ( $-4$  to  $243 \text{ kg m}^{-2} \text{ a}^{-1}$ ), with a standard deviation of 59%. The higher accumulation and lower standard deviation may be correlated to the weak impact of wind scouring.

**Zone 5:** The Dome A area (1128–1246 km) has the lowest average accumulation rate,  $35 \text{ kg m}^{-2} \text{ a}^{-1}$  (11 cm of snow), and a moderate variability ( $-1$  to  $109 \text{ kg m}^{-2} \text{ a}^{-1}$ ), with a standard deviation of 54%, due to a low and varying wind speed.

Precipitation/SMB is controlled by air masses and topography (Noone and others, 1999; Frezzotti and others, 2004). The SMB variability in this area mainly reflects ablation processes driven by katabatic winds. In section 3, we discussed how wind speed and direction change. In Table 3 and Figures 3 and 5, the annual average snow accumulation is shown to have an apparent positive correlation with slope due to direct influence of katabatic wind speed. To test this correlation, we used regression analyses and found that the  $R^2$  value of the standard deviation of snow accumulation with slope is 0.76. Strong wind has a positive relationship with the standard deviation of snow accumulation, because it redeposits the surface snow and produces sastrugi and wind crust (Xiao and others, 2005). Scarchilli and others (2010) point out that the combined processes of blowing-snow sublimation and snow transport remove (mainly in the atmosphere) up to 50% of precipitation in the coastal and slope convergence area. Solar forcing is an important factor influencing the SMB by inducing surface sublimation (Qin, 1995). There is insufficient information from the transect on solar forcing, but we have reason to believe that the wind is the most important factor, because it not only moves snow but also contributes to sublimation.

### 4.3. Temporal variability of surface mass balance

Measurements of the stake arrays show temporal variations of SMB (Table 1; Fig. 4). DT008, which is 310 km from the coast, had an accumulation rate of  $138 \text{ kg m}^{-2} \text{ a}^{-1}$  during 1998–2005 and of  $80 \text{ kg m}^{-2} \text{ a}^{-1}$  during 2005–08, a decrease of  $\sim 40\%$ . DT217, DT364 and DT401 exhibited values of 11, 56 and  $25 \text{ kg m}^{-2} \text{ a}^{-1}$  respectively during 1998/99–2005, and 12, 72 and  $28 \text{ kg m}^{-2} \text{ a}^{-1}$  during 2005–08, increases of 10%, 29% and 14%, respectively, suggesting similar temporal climatological variability. Dome A also had an increase of 16%, but the time-span of the data for this site is short, restricting their reliability. The annual accumulation rate is  $19 \text{ kg m}^{-2} \text{ a}^{-1}$ , much lower than that of Dome Fuji ( $27 \text{ kg m}^{-2} \text{ a}^{-1}$ ; Kameda and others, 2008). Another interesting phenomenon is that the areas with higher accumulation experienced greater changes.

Although all the distribution curves (Fig. 4) are wider for 1999–2005 and more negative values are shown for 2005–08, this does not mean that the surface morphology has recently become more variable; rather, the multi-year data smoothed the local noise.

In section 4.2 we discussed the regional-scale spatial variability of SMB and demonstrated that there were high standard deviations for all zones; we are unable to estimate the temporal changes from the coast to 68 km and from 1128 to 1246 km due to insufficient data. However, the average accumulation rate from 68 to 202 km decreased from  $615 \text{ kg m}^{-2} \text{ a}^{-1}$  (1997–98) to  $157 \text{ kg m}^{-2} \text{ a}^{-1}$  (2005–08) (Table 3). This is in contrast to Ren and others (2002b), who observed an increasing trend from 1994 to 1999 in the same zone. In zone 2, the accumulation rate decreased from 84 to  $67 \text{ kg m}^{-2} \text{ a}^{-1}$  from 1999–2005 to 2005–08. During the same period, the accumulation rate over the next two zones increased from 59 to  $65 \text{ kg m}^{-2} \text{ a}^{-1}$ . There was no change in the 202–1128 km sector ( $65.5 \text{ kg m}^{-2} \text{ a}^{-1}$ ) from 1999–2005 to 2005–08. That is, the SMB of the eastern side of the LGB was stable, with the annual accumulation rate decreasing in the coastal area yet increasing inland.

## 5. CONCLUSION

Stake measurements reveal a detailed spatial distribution of SMB along the traverse route from Zhongshan to Dome A. Slope and wind speed correlate positively with the standard deviation of snow accumulation, which reflects the roughness of the snow surface. Zone 1 has the highest snow accumulation rate and lowest spatial variability due to having the highest precipitation, linked to incoming marine air masses in that area. The slowly rising area, zone 2, is a transition zone between the coast and inland. Zone 3 has a relatively low accumulation rate ( $52 \text{ kg m}^{-2} \text{ a}^{-1}$ ) and more compact surface snow due to high wind speeds. The surface morphology of zone 4 is very complex; its accumulation rate and spatial variability are higher than those of adjacent areas. Zone 5, the Dome A area, has the lowest accumulation rate and moderate spatial variability because it is the highest zone and furthest from the coast, and has the lowest wind speed.

The accumulation pattern derived from the stake arrays and sastrugi height suggests that the local annual noise in snow accumulation has a significant impact on net accumulation records, so a single stake or ice/firn core provides only limited local representation. The highest standard deviation values occur in areas of high ablation and lower accumulation. The two lowest standard deviations (stake arrays at

DT364 and Dome A) are in areas with low wind speeds or high precipitation.

Over the past decade, the SMB of the eastern side of the LGB has been stable. Although there are not enough data to analyse the entire transect, it appears that the accumulation rate in the inland area increased. One explanation is that air masses may transfer moisture inland more easily due to climate warming (Solomon and others, 2007). More field-work needs to be carried out around the Dome A area to confirm this trend.

The area from 250 to 400 km exhibits a decreasing trend in accumulation rate over the past decade, which is also observed in other areas (at equal distances from the coast) throughout the East Antarctic ice sheet. It has previously been reported that the western side of the LGB has a temporal trend opposite to that of the eastern side (Ren and others, 2002b), so further work on the western side of the LGB is required. Due to the extreme environment and extent of Antarctica, the extrapolation of SMB in large regions is only possible through the integration of extensive field observation and remote-sensing and/or climate-modelling interpolation methods.

## ACKNOWLEDGEMENTS

We thank CHINARE for logistical support. This study was funded by the National Natural Science Foundation of China (500222103002, 40825017), the Hundred Talent Project of the Chinese Academy of Sciences, and the Natural Science Project of the Ministry of Science and Technology of the People's Republic of China (2006BAB18B01). We also received logistical and financial support from the Chinese Arctic and Antarctic Administration and the State Key Laboratory of Cryospheric Sciences. We thank all members of the traverse teams. We also thank J. Ming and M. Frezzotti for many helpful comments.

## REFERENCES

- Allison, I. 1998. Surface climate of the interior of the Lambert Glacier basin, Antarctica, from automatic weather station data. *Ann. Glaciol.*, **27**, 515–520.
- Connolley, W.M. and J.C. King. 1996. A modeling and observational study of East Antarctic surface mass balance. *J. Geophys. Res.*, **101**(D1), 1335–1344.
- Dibb, J.E. and M. Fahnestock. 2004. Snow accumulation, surface height change, and firn densification at Summit, Greenland: insights from 2 years of in situ observation. *J. Geophys. Res.*, **109**(D24), D24113. (10.1029/2003JD004300.)
- Ding, M., C. Xiao, B. Jin, J. Ren, D. Qin and W. Sun. 2010. Distribution of  $\delta^{18}\text{O}$  in surface snow along a transect from Zhongshan Station to Dome A, East Antarctic. *Chinese Sci. Bull.*, **55**(24), 2709–2714.
- Eisen, O. and 15 others. 2008. Ground-based measurements of spatial and temporal variability of snow accumulation in East Antarctica. *Rev. Geophys.*, **46**(RG2), RG2001. (10.1029/2006RG000218.)
- Frezzotti, M., S. Gandolfi, F. La Marca and S. Urbini. 2002a. Snow dunes and glazed surfaces in Antarctica: new field and remote-sensing data. *Ann. Glaciol.*, **34**, 81–88.
- Frezzotti, M., S. Gandolfi and S. Urbini. 2002b. Snow megadunes in Antarctica: sedimentary structure and genesis. *J. Geophys. Res.*, **107**(D18), 4344. (10.1029/2001JD000673.)
- Frezzotti, M. and 12 others. 2004. New estimations of precipitation and surface sublimation in East Antarctica from snow accumulation measurements. *Climate Dyn.*, **23**(7–8), 803–813.

- Frezzotti, M. and 13 others. 2005. Spatial and temporal variability of snow accumulation in East Antarctica from traverse data. *J. Glaciol.*, **51**(172), 113–124.
- Frezzotti, M., S. Urbini, M. Proposito, C. Scarchilli and S. Gandolfi. 2007. Spatial and temporal variability of surface mass balance near Talos Dome, East Antarctica. *J. Geophys. Res.*, **112**(F2), F02032. (10.1029/2006JF000638.)
- Furukawa, T., K. Kamiyama and H. Maeno. 1996. Snow surface features along the traverse route from the coast to Dome Fuji Station, Queen Maud Land, Antarctica. *Proc. NIPR Symp. Polar Meteorol. Glaciol.*, **10**, 13–24.
- Goodwin, I.D. 1991. Snow-accumulation variability from seasonal surface observations and firn-core stratigraphy, eastern Wilkes Land, Antarctica. *J. Glaciol.*, **37**(127), 383–387.
- Goodwin, I., H. De Angelis, M. Pook and N.W. Young. 2003. Snow accumulation variability in Wilkes Land, East Antarctica and the relationship to atmospheric ridging in the 130°–170° E region since 1930. *J. Geophys. Res.*, **108**(D21), 4673. (10.1029/2002JD002995.)
- Hou, S., Y. Li, C. Xiao and J. Ren. 2007. Recent accumulation rate at Dome A, Antarctica. *Chinese Sci. Bull.*, **52**(3), 428–431.
- Jacobs, S.S., H.H. Hellmer, C.S.M. Doake, A. Jenkins and R.M. Frolich. 1992. Melting of ice shelves and the mass balance of Antarctica. *J. Glaciol.*, **38**(130), 375–387.
- Kameda, T., H. Motoyama, S. Fujita and S. Takahashi. 2008. Temporal and spatial variability of surface mass balance at Dome Fuji, East Antarctica, by the stake method from 1995 to 2006. *J. Glaciol.*, **54**(184), 107–116.
- Ma, Y., L. Bian, C. Xiao, I. Allison and X. Zhou. 2010. Near surface climate of the traverse route from Zhongshan Station to Dome A, East Antarctica. *Antarct. Sci.*, **22**(4), 443–459.
- McConnell, J.R., R.C. Bales and D.R. Davis. 1997. Recent intra-annual snow accumulation at South Pole: implications for ice core interpretations. *J. Geophys. Res.*, **102**(D18), 21,947–21,954.
- Noone, D., J. Turner and R. Mulvaney. 1999. Atmospheric signals and characteristics of accumulation in Dronning Maud Land, Antarctica. *J. Geophys. Res.*, **104**(D16), 19,191–19,211.
- Qin, D. 1995. The physical process in the shallow surface layer of the Antarctic ice sheet. In Qin, D. *A study of present climatic and environmental record in the surface snow of the Antarctic ice sheet*. Beijing, Science Press, 32–59. [In Chinese.]
- Ren, J. and D. Qin. 1995. A study of snow stratigraphy and accumulation-rate change in the west part of the Lambert Glacier basin, East Antarctica. *J. Glaciol. Geocryol.*, **17**(3), 274–282. [In Chinese with English summary.]
- Ren, J. and D. Qin. 1996. Surface accumulation rate and mass balance of the Antarctic Ice Sheet. *J. Glaciol. Geocryol.*, **18**(51), 83–89. [In Chinese.]
- Ren, J., D. Qin, I. Allison, M. Higham and I.D. Goodwin. 1995. A study of snow stratigraphy and accumulation-rate change in the west part of the Lambert Glacier basin, East Antarctica. *J. Glaciol. Geocryol.*, **17**(3), 274–282. [In Chinese with English summary.]
- Ren, J., D. Qin and C. Xiao. 2001. Preliminary results of the inland expeditions along a transect from the Zhongshan Station to Dome A, East Antarctica. *J. Glaciol. Geocryol.*, **23**(1), 51–56. [In Chinese with English summary.]
- Ren, J., C. Xiao, D. Qin and J. Sun. 2002a. Mass balance in the Lambert Glacier Basin and variability of the Antarctic Ice Sheet. *Progr. Natur. Sci.*, **12**(10), 1064–1069. [In Chinese.]
- Ren, J., I. Allison, C. Xiao and D. Qin. 2002b. Mass balance of the Lambert Glacier basin, East Antarctica. *Sci. China D*, **45**(9), 842–850.
- Scarchilli, C., M. Frezzotti, P. Grigioni, L. De Silvestri, L. Agnoletto and S. Dolci. 2010. Extraordinary blowing snow transport events in East Antarctica. *Climate Dyn.*, **34**(7–8), 1195–1206.
- Slonaker, R. and M.L. Van Woert. 1999. Atmospheric moisture transport across the Southern Ocean via satellite observations. *J. Geophys. Res.*, **104**(D8), 9229–9249.
- Solomon, S. and 7 others, eds. 2007. *Climate change 2007: the physical science basis. Contribution of Working Group I to the Fourth Assessment Report of the Intergovernmental Panel on Climate Change*. Cambridge, etc., Cambridge University Press.
- Takahashi, S. and T. Kameda. 2007. Snow density for measuring surface mass balance using the stake method. *J. Glaciol.*, **53**(183), 677–680.
- Urbini, S. and 6 others. 2008. Historical behaviour of Dome C and Talos Dome (East Antarctica) as investigated by snow accumulation and ice velocity measurements. *Global Planet. Change*, **60**(3–4), 576–588.
- Xiao, C., D. Qin, L. Bian, X. Zhou, I. Allison and M. Yan. 2005. A precise monitoring of snow surface height in the region of Lambert Glacier basin–Amery Ice Shelf, East Antarctica. *Sci. China D*, **48**(1), 100–111.
- Xiao, C., Y. Li, S. Hou, I. Allison, B. Lingen and J. Ren. 2008. Preliminary evidence indicating Dome A (Antarctica) satisfying preconditions for drilling the oldest ice core. *Chinese Sci. Bull.*, **53**(1), 102–106. [In Chinese.]
- Zhang, S., D. E, Z. Wang, C. Zhou and Q. Shen. 2007. Correspondence. Surface topography around the summit of Dome A, Antarctica, from real-time kinematic GPS. *J. Glaciol.*, **53**(180), 159–160.

MS received 29 September 2010 and accepted in revised form 2 March 2011